Journal of Alloys and Compounds 509 (2011) 387–390

Contents lists available at ScienceDirect

Journal of Alloys and Compounds

journal homepage: www.elsevier.com/locate/jallcom

Hydrothermal synthesis and optical properties of Ni doped ZnO hexagonal nanodiscs

T. Al-Harbi*

King Abdul-Aziz University, Faculty of Science, Physics Department, Jeddah, Saudi Arabia

ARTICLE INFO

Article history:
Received 11 August 2010
Received in revised form 2 September 2010
Accepted 3 September 2010
Available online 16 September 2010

Keywords:
Doping
Nanostructures
Hydrothermal crystal growth
Semiconducting materials

ABSTRACT

Single crystalline Ni-doped ZnO hexagonal nanodiscs are successfully synthesized. Zinc acetate, nickel nitrate, sodium hydroxide and poly (vinyl pyrrolidone) (PVP) were mixed together and transferred to a 100 ml Teflon-lined stainless steel autoclave which kept at 150 °C for 24 h. The morphology and microstructure were determined by field emission scanning electron microscopy (FE-SEM), X-ray diffraction transmission electron microscopy (TEM), energy-dispersive X-ray spectroscopy (EDX) and photoluminescence (PL) spectroscopy. The investigation confirmed that the products were of the wurtzite structure of ZnO. The doped hexagonal nanodiscs have edge length 30 nm and thickness of 45 nm. EDX result showed that the amount of Ni in the product is about 12%. Photoluminescence of these doped hexagonal nanodiscs exhibits a blue shift and weak ultraviolet (UV) emission peak, compared with pure ZnO, which may be induced by the Ni-doping. The growth mechanism of the doped hexagonal nanodiscs was also discussed.

1. Introduction

Synthesis of size and shape controlled metal oxide nanostructures is very important in controlling their physical and chemical properties, and crucial for their potential uses. Recently, considering the properties of the materials are greatly affected by their morphologies, wide range of metal oxide with different morphologies providing great opportunities for the discovery of new properties and potential uses have been synthesized via different methods. Among these methods, hydrothermal approach [1,2] has great advantages in synthesizing metal oxide crystals through relative low temperature and simple equipment, which makes the method more suitable and economic for large-scale production. In order to control the morphology of ZnO crystals, organic additives: such as PVP, PEG, SDS and CTAB [3–5], were commonly introduced into the reaction system to manipulate the nucleation and growth in hydrothermal reactions. However, it still remains a challenge to understand their precise working mechanism in directing the growth of ZnO.

As an important II–VI semiconductor, ZnO has a wide band gap (3.37 eV) and large exciton binding energy of 60 meV [6]. Therefore, it is a promising material for the fabrication of optoelectronic devices operating in the blue and ultraviolet (UV) region [7]. Moreover, due to its superior conducting properties, ZnO has also been investigated as a transparent conducting and piezoelectric material for use as electrodes, catalysts and sensors [8]. Recently, various doped ZnO nanostructures with different elements have been achieved to improve the electrical, optical and magnetic properties [9].

Nanosized nickel oxide has demonstrated excellent properties such as catalytic [10], magnetic [11], electrochromic [12], optical and electrochemical properties [13]. Furthermore, nickel oxides can be used as a transparent p-type semiconducting layer [14] and are being studied for applications in smart windows, electrochemical supercapacitors [15] and dye sensitized photocathodes [16].

The aim of the present contribution is the investigation of structures and optical properties of Ni-doped ZnO hexagonal nanodiscs, which is very important for both fundamental and applied points of view.

2. Experimental work

For the synthesis of Ni doped ZnO nanopowders, analytical grade zinc acetate dehydrate [$Zn(O_2CCH_3)_2(H_2O)_2$], nickel nitrate [$Ni(NO_3)_3{\cdot}6H_2O$], sodium hydroxide (NaOH) and poly vinyl alcohol (PVA) were used. All the reagents were used as received (Fluka and Aldrich) without further purification. In a typical reaction process for the growth of hexagonal nano-discs Ni doped ZnO, 1.975 g zinc acetate dehydrate, 0.305 g of nickel nitrate and 3.0 g of PVP were dissolved in 100 ml deionized water and stirred for 30 min. Simultaneously, a 10 ml NaOH (10 M) was added drop wise into this aqueous zinc acetates, nickel nitrate and PVP solution under vigorous stirring. During the addition of NaOH into aqueous solution, the solution was heated at 80 °C to avoid the immediate precipitation of zinc and nickel ions. At last, the final solution was transferred into a 100 ml Teflon-lined stainless steel autoclave. The autoclave was sealed and maintained at 150 °C for 24 h, and then allowed to cool to room temperature naturally. After terminating the reaction in desired

* Tel.: +966 50680787.
E-mail address: tharbi1@yahoo.com.

0925-8388/$ – see front matter © 2010 Elsevier B.V. All rights reserved.
doi:10.1016/j.jallcom.2010.09.034

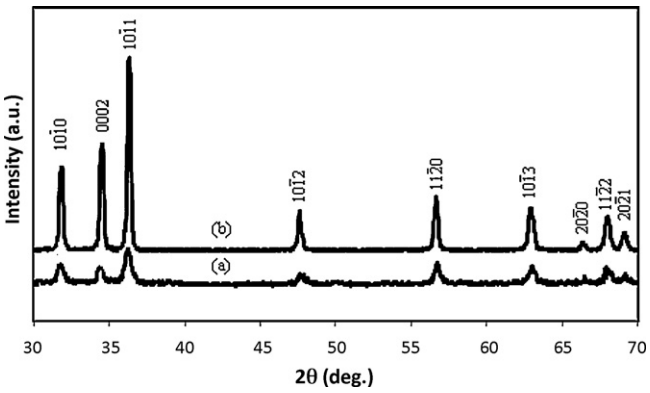

Fig. 1. XRD pattern of (a) Ni doped ZnO and (b) ZnO.

time, the resulted solid projects were centrifuged, washed with distilled water and ethanol to remove the ions possibly remaining in the final product, and finally dried in vacuum at 60 °C for 4 h. The synthesized Ni doped ZnO hexagonal-nanodiscs were characterized in terms of their structural and optical.

The X-ray measurements were performed using Philips X'pert diffractometer supplied with copper X-ray tube ($\lambda_{k\alpha1}$ = 1.5406 Å), nickel filter, graphite crystal monochromator, proportional counter detector, divergence slit 1° and 0.1 mm reNi-iving slit. The working conditions were 40 kV and 30 mA for the X ray tube, scan speed 0.05° and 2 s measuring time per step. For each measurement, a complete scan was made between 10° and 70° (2θ°). To calibrate the measured Bragg 2θ-angles, a standard referenNi material (SRM 640a) of pure Si powder was used.

High resolution transmission electron microscopy (HR-TEM) of purified ZnO and Ni doped ZnO nanopowders was carried out using a JEOL 2010 high-resolution transmission electron microscope operated at 200 kV. To prepare the HRTEM samples, purified ZnO and Ni doped ZnO nanopowders were first redispersed in ethanol and diluted, followed by placing a droplet of the solution onto a 400-mesh carbon-coated copper grid. The grid was then dried in desiccators for one day before imaging. The photoluminescence was measured at room temperature by He–Cd laser with a wavelength 325 nm as the excitation source. This measurement was carried out by preparing dilute solution of ZnO and Ni doped ZnO nanopowders in ethanol.

3. Results and discussion

Fig. 1 shows the XRD patterns of the grown Ni doped ZnO nanostructures before and after calcination. The grown nanostructures show several peaks of (1 0 −1 0), (0 0 0 2), (1 0 −1 1), (1 1 −2 0), (1 0 −1 3), (2 0 −2 0), (1 1 −2 2) and (2 0 −2 1), no signals of the metallic Zn are detected by XRD. Also, there are no peaks corresponding with the Ni or its oxides, suggesting that the Ni element may be doped into ZnO. The high intensities of calcined nanostructure peaks with narrower width reveal a highly crystallized wurtzite structure. The size of the Ni doped ZnO nanoparticles was estimated by applying the Scherrer equation [17] to the half intensity width of the (1 0 −1 0), (0 0 0 2) and (1 0 −1 1) peaks:

$$d = \frac{k\lambda}{\beta \cos\theta} \quad (1)$$

where k is the particle shape factor and taken as 0.827 because of the hexagonal NiZnO nanoparticles as shown in Fig. 2a, λ is the wavelength of Cu Kα radiation (0.154 nm), β is the calibrated half intensity width of the selected diffraction peak (degrees), and θ is the Bragg angle (half of the peak position angle). From this equation, the average size of the Ni-doped ZnO nanoparticles was estimated to be approximately 58 nm and thickness about 45 nm.

When only ZnO was synthesized under same conditions, the undoped ZnO powder with white color is nanorod-shaped, with length 120 nm and diameter 18 nm, and each rod crystal extends along the c-axis of the wurtzite structure as indicated in Fig. 2, while the Ni-doped ZnO powder showed hexagonal-like nanodiscs with an average size of approximately 60 nm, as shown in Fig. 3c. They are in a fine dispersion, unagglomerated, and have a distinct surface thought to consist of {0 0 0 1} plane. In addition, the color of the Ni-doped ZnO nanoparticles is not white but bright green. These imply that the Ni element has been doped into the ZnO lattice and controls the ZnO growth.

Fig. 3a reveals the magnified image of a single regularly hexagonal Ni-doped ZnO nanodisc with average edge length of about 30 nm and thickness up to about 45 nm. The content of Ni element measured by EDX was about 12% as shown in Fig. 3d.

HRTEM image of the regularly hexagonal nanoparticle shown in Fig. 3b clearly indicates the two-dimensional lattice fringe of the wurtzite structure without any small area of zinc blend in this particle. The hexagonal nanoparticle is a perfect single crystal without any defects such as the dislocations and twins. It is worth noticing that the distance (0.28 nm) between two neighboring (1 −1 0 0) planes in the Ni-doped ZnO nanoparticle is larger than that (0.26 nm) of the undoped ZnO nanoparticle, i.e. there is an increase of 7.6% for the $d_{(1\,-1\,0\,0)}$ value for the Ni-doped ZnO nanoparticle. This is another proof that the Ni element has been doped into the lattice of the ZnO nanoparticles. The spot diffraction pattern (inset of Fig. 3b) further confirmed the XRD result that the Ni-doped ZnO nanoparticles have the highly crystallized wurtzite structure (h.c.p. crystal).

The possible mechanism of the formation of hexagonal Ni doped ZnO hexagonal nanodiscs can be discussed based on both of its internal structure (effect of adding Ni element) and the capping ligands (PVP). It is well known that the synthesis of NCs includes two steps: nucleation and growth. At the nucleating stage, the intrinsic crystal properties dominate the shape of the initial NiZnO seeds, that is, platelet seeds. Subsequently, the precursors are absorbed to each plane, and the seed grows with different rates along different planes. Actually, PVP is very important in the preparation of isotropic Ni doped ZnO hexagonal nanodiscs, PVP as capping ligands can change the surface energy of different crystal facets, the side facets may possess higher energy than the top-down surfaces, thus ultimately leading to the formation of Ni doped ZnO nanodiscs. Matysina [18] determined that hexagonal metals with c/a ratios greater than 1.633 have {1 0 1} and {1 0 0} surface energy 1.5 times larger than those for {0 0 1} facets [16]. Ni doped ZnO has a c/a ratio of 2.6 and should have even higher surface energy on the {1 0 1} and {1 0 0} surfaces. As a result, the Ni doped ZnO nanodisc grows more rapidly along these facets, and the [1 1 0] direction is the long axis of the nanodisc while the [0 0 1] direction is the short axis. On the other hand, Muthukumar et al. [19] found that the N doped into the ZnO films could control the surface morphology by lowering the surface energy. It may be speculated that the Ni element doped into the crystal lattice of the Zn embryos lowers the surface energy of the {1 0 −1 0} planes, resulting in an isotropic oxidation growth of the Zn embryos instead of the preferred growth at (1 0 −1 0). At the same time, the completely oxidized embryos may coalesce Ni each other with the definite direction (1 0 −1 0) and the regularly hexagonal Ni-doped ZnO nanoparticles are synthesized. Therefore, the formation of the Ni-doped ZnO nanoparticles may be controlled by the Ni doped into the lattice of the Zn embryos.

Fig. 4 depicts the PL spectra of the pure ZnO and Ni-doped ZnO hexagonal nanodiscs excited by 325 nm at room temperature. The PL spectra of pure ZnO nanodiscs have a strong UV band peak at 380 nm. Besides, a relatively strong and broad green band centered at about 510 nm occurred. The UV emission resulted from excitonic recombination corresponding to the near band-edge emission of ZnO. The green emission peak is originated due to deep-level or trap-state emission [20,21]. In fact, there are different mechanisms have been proposed for the visible light emission of ZnO. Oxygen vacancies occur in three different charge states: the neutral oxygen vacancy, the singly ionized oxygen vacancy and the doubly ionized oxygen vacancy [22]. Van heusden et al. [23] found that only the singly ionized oxygen vacancies are responsible for the green luminescence in the ZnO. Compared with the PL spectrum

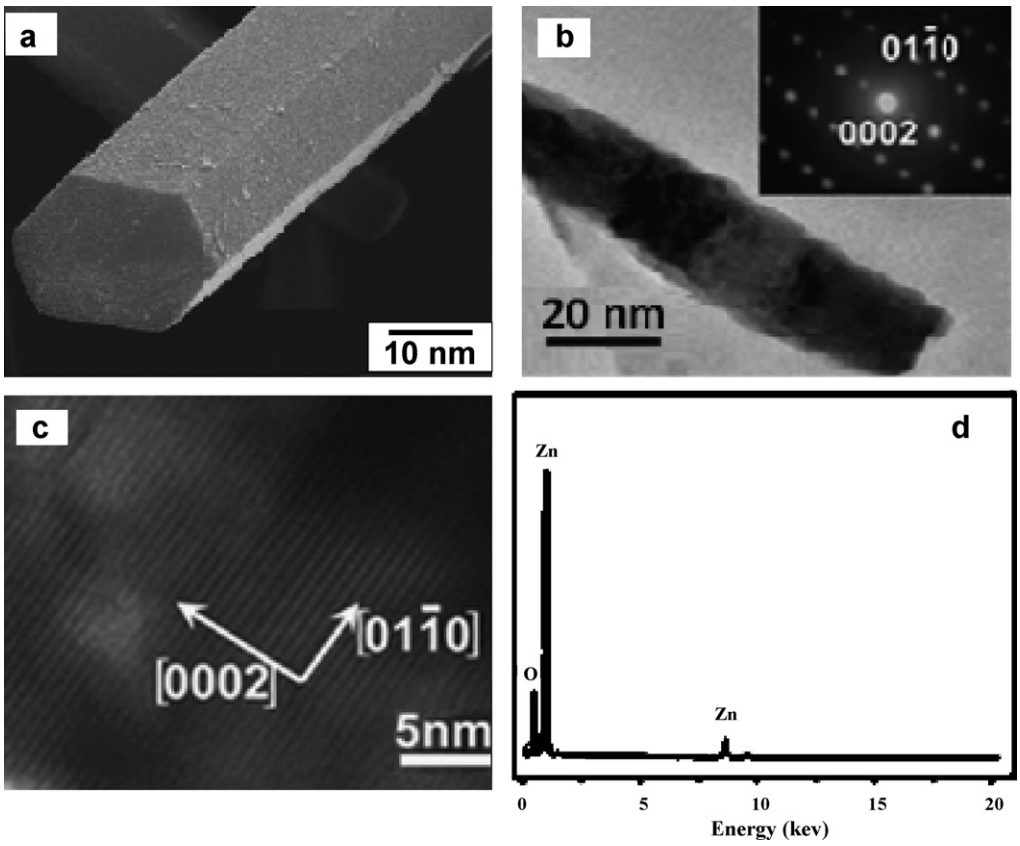

Fig. 2. (a) High magnification SEM micrograph of the ZnO nano-hexagonal rod, (b) HRTEM image of the ZnO nanorods (inset diffraction pattern), (c) SAED and (d) EDX.

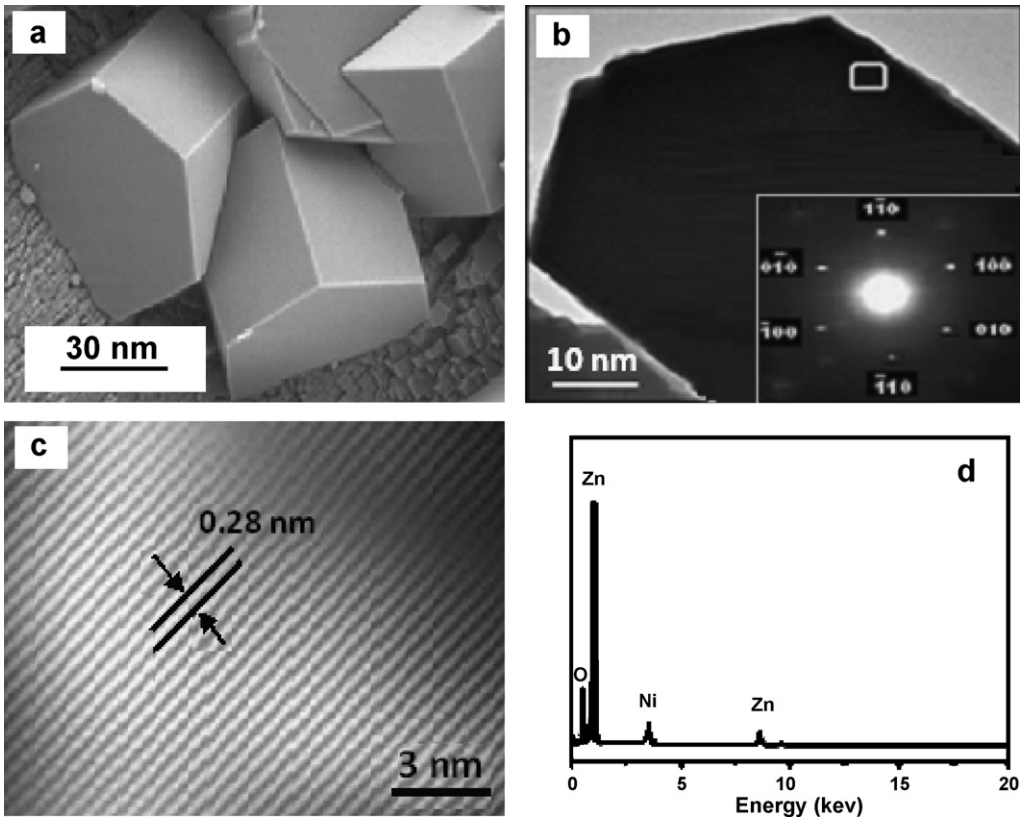

Fig. 3. (a) High magnification SEM micrograph of the Ni doped ZnO hexagonal disc, (b) HRTEM image of the Ni doped ZnO nanodisc (inset diffraction pattern), (c) SAED and (d) EDX.

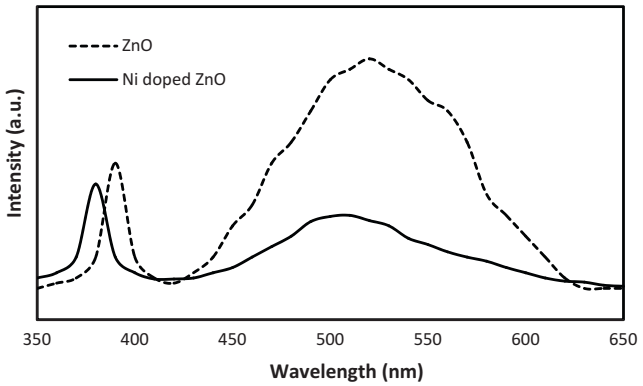

Fig. 4. PL of pure ZnO and Ni doped ZnO hexagonal nanodiscs at room temperature.

of ZnO nano-disc, the peak position of UV emission, for Ni-doped ZnO nano-disc, exhibits blue shift while the green emission band is sharply suppressed. For Ni doped ZnO nano-disc, more electrons contributed by nickel dopants would take up the energy levels located at the bottom of conduction band. When they were excited by the laser of 325 nm, the excitons take up higher energy levels at the bottom of conduction band. Radioactive recombination of these excitons will lead to a blue shift and broaden of UV emission peak [24]. The lattice strain induced by the lattice distance would also lead to some shift in band gap but may not play a major role in the determination of band gap as the small deformation of the lattice distances. Decreased UV emission was considered due to the increase of the nano-radiative defects and decrease of ZnO nano-disc size [25]. A blue shift of the band edge revealed from PL points to the incorporation of at least a part of Ni on the lattice sites. This supports the X-ray results on the incorporation of Ni into the nano-disc structure. When Ni ions are incorporated into ZnO and become donors, multi-emission centers are formed, such as the emission of the electron–hole plasma (EHP), the emission of the donors to the valence band, and the intrinsic transition of Ni^{3+} ions [26]. So the green emission of Ni doped ZnO nanodiscs was more broad than the undoped. The PL integrated intensity ratio of the UV emission to the deep-level green emission (I_{UV}/I_{DLE}) is 0.6 and 1.3, for ZnO and Ni-doped ZnO nanodiscs, respectively. Generally, the intensity ratio of UV emission band to visible emission band is regarded as an indicator of the crystal of ZnO materials. The strong UV and weak green bands imply good crystal surface [27]. The increased ratio suggests the good crystal of Ni-doped ZnO nanodiscs. These results showed a great promise for the Ni-doped ZnO nanodiscs with applications in optoelectronic devices.

4. Conclusion

Single crystalline Ni doped ZnO hexagonal nanodiscs were successfully synthesized using polymer as a surfactant. The calcined Ni-doped ZnO powder is the hexagonal nanoparticles with an average of about 52 nm in a narrow distribution. XRD, HRTEM, SAED and EDX analysis results clearly show that the Ni element has been doped into the ZnO crystal lattice and no metallic Zn as well as Ni exists in the Ni-doped ZnO nanoparticles. The Ni ions doped into the ZnO crystal lattice may be responsible for the morphology of the Ni-doped ZnO nanoparticles due to minimize the surface energy of the preferred growth planes $\{1\,0\,-1\,0\}$. A strong UV emission and a weak broad green emission band with peaks centering at 380 and 510 nm were observed at room temperature. It should be emphasized that the strong UV and weak green bands imply good crystal surface. The increased ratio suggests the good crystal of Ni-doped ZnO nanodiscs. These results showed a great promise for the Ni-doped ZnO nanodiscs with applications in optoelectronic devices.

Acknowledgment

Thanks for Dr. Waleed E Mahmoud for his kind help and valuable discussion during working on this research.

References

[1] L. Vayssieres, Adv. Mater. 15 (2003) 464.
[2] M. Guo, P. Diao, S. Cai, J. Solid State Chem. 178 (2005) 1864.
[3] X.M. Sui, Y.C. Liu, C.L. Shao, Chem. Phys. Lett. 424 (2006) 340.
[4] X.F. Zhou, Z.L. Hu, Y. Chen, H.Y. Shang, Mater. Res. Bull. 43 (2008) 2790.
[5] T. Pauporte, J. Rathousky, Micropor. Mesopor. Mater. 117 (2009) 380.
[6] Y. Peng, L. Bao, Front. Chem. China 4 (2008) 458.
[7] H. Cao, J.Y. Xu, D.Z. Zhang, S.H. Chang, S.T. Ho, E.W. Seelig, X. Liu, R.P.H. Chang, Phys. Rev. Lett. 84 (2000) 5584.
[8] Y.S. Chen, T.Y. Tseng, J. Nanosci. Nanotechnol. 8 (9) (2008) 4514.
[9] G.D. Yuan, W.J. Zhang, J.Sh. Jie, X. Fan, J.X. Tang, Ch.S. Lee, Sh.T. Lee, Adv. Mater. 20 (2008) 168.
[10] Y. Wang, J. Zhu, X. Yang, L. Lu, X. Wang, Thermochim. Acta 437 (2005) 106.
[11] Y.R. Uhm, J.H. Park, W.W. Kim, C.H. Cho, C.K. Rhee, Mater. Sci. Eng. B 106 (2004) 224.
[12] S.H. Lin, F.R. Chen, J.J. Kai, Appl. Surf. Sci. 254 (2008) 3357.
[13] X. Wang, J. Song, L. Gao, J. Jin, H. Zheng, Z. Zhang, Nanotechnology 16 (2005) 37.
[14] H. Sato, T. Minami, S. Takata, T. Yamada, Thin Solid Films 236 (1993) 27.
[15] V. Srinivasan, J. Weidner, J. Electrochem. Soc. 144 (1997) L210.
[16] J. He, H. Lindström, A. Hagfeldt, S.E. Lindquist, J. Phys. Chem. B 103 (1999) 8940.
[17] W.E. Mahmoud, A.A. Al-Ghamdi, F. El-Tantawy, S. Al-Heniti, J. Alloys Compd. 485 (2009) 59–63.
[18] Z.A. Matysina, Mater. Chem. Phys. 60 (1999) 70.
[19] S. Muthukumar, C.R. Gorla, N.W. Emanetoglu, S. Liang, Y. Lu, J. Cryst. Growth 197 (2001) 225.
[20] N. Kumar, A. Dorfman, J. Hahm, J. Nanosci. Nanotechnol. 5 (2005) 1915.
[21] D.M. Bagnall, Y.F. Chen, M.Y. Shen, Z. Zhu, T. Goto, T. Yao, J. Cryst. Growth 184 (1998) 605.
[22] J. Jie, G. Wang, X. Han, Q. Yu, Y. Liao, G. Li, J.G. Hou, Chem. Phys. Lett. 387 (2004) 466.
[23] K. Vanheusden, C.H. Seager, W.L. Warren, D.R. Tallent, J.A. Voigt, J. Appl. Phys. 79 (1996) 7983.
[24] A.K. Pradhan, T.M. Williams, K. Zhang, D. Hunter, J.B. Dadson, K. Lord, U.N. Roy, Y. Cui, A. Burger, J. Nanosci. Nanotechnol. 6 (2006) 1985.
[25] A. Umar, S.H. Kim, Y.S. Lee, K.S. Nahm, Y.B. Hahn, J. Cryst. Growth 282 (2005) 131.
[26] B. Cheng, Y. Xiao, G. Wu, L. Zhang, Adv. Funct. Mater. 14 (9) (2004) 913.
[27] U. VeaNislav, R. Emil, Z. Victor, S. Lilian, M. Eduard, T. Ion, Inform. Technol. 5822 (2005) 148.